



Yield stress measurement of a thixotropic colloid

Ernest E. S. Ong¹ · Sean O'Byrne¹ · Jong Leng Liow¹

Received: 5 February 2019 / Revised: 2 May 2019 / Accepted: 22 May 2019 / Published online: 8 June 2019
© Springer-Verlag GmbH Germany, part of Springer Nature 2019

Abstract

Yield stress measurements have long been considered to be inconsistent and difficult, especially for a thixotropic colloid, since the thixotropic behavior gives rise to time-dependent rheological properties. In this paper, we attempted measuring the yield stress of aqueous xanthan gum (XG) solutions in different XG concentration. Our rheological measurements showed that XG in aqueous solutions, which can be characterized as weak gels, were thixotropic for 0.4, 0.6, 0.8, and 1 wt% XG concentrations. To ensure the accuracy of our rheological measurement data, detailed wall slip and stress relaxation time were first investigated prior to the actual yield stress measurement. A standard sample loading procedure was used to ensure the consistency of the loaded sample. Various methods were employed such as steady shear, oscillatory shear, rheological model fitting, and creep test to determine the yield stress of aqueous XG solutions. A sigmoidal model was also proposed to obtain a yield stress from our steady shear measurement unambiguously. In our steady shear measurements, a resistance to an avalanche of flow is observed and it is likely due to a conformational change of XG polymers under shear. As compared to other measurement methods, it was found that the most reliable way to obtain a yield stress is via small amplitude oscillatory shear measurements, in which a yield stress can be obtained conveniently at the maximum storage modulus, and it is well matched with our steady shear and creep test results.

Keywords Yield stress · Xanthan gum · Thixotropy · Polymer solution · Shear-induced conformational change

Introduction

A yield stress fluid (YSF) is a viscoelastic material that behaves like an elastic solid under low shear stresses, and flows like a viscous liquid when its critical shear stress is exceeded. A thixotropic colloid, like mayonnaise, is a typical example of a YSF. It does not flow and behaves like a solid when there are no forces acting upon it, whereas it spreads out and flows readily when a sufficiently large force is applied to it. The idea of a yield stress was quite controversial in the past (Barnes and Walters 1985; Barnes 1999) but it is now generally accepted. A precise quantitative knowledge of yield stress is important in the handling, storage, processing, and transportation of YSFs in various industries (Castro et al. 2010; Dzuy and Boger 1983). In the mining industry, for example, yield stress is an important factor in the design of pipelines and pumps

(Chang et al. 1999; Dzuy and Boger 1983; Mendes et al. 2016; Norrman et al. 2016) as well as on-site operations like oil well drilling (Balhoff et al. 2011). In the oil industry during a shut-in and restart operation, the crude oil flow in pipelines could be initiated only after several days or weeks of continuous inlet pressure application (Norrman et al. 2016). If the rheological properties (including yield stress) of complex waxy crude oil were well understood, the issue of lost production time would be minimized. In addition, yield stress is also important in the design of nuclear waste sludge disposal (Botha et al. 2016; Gens et al. 2009). In the construction industry, the productivity and quality of cement and concrete is very much related to yield stress (Chidiac and Mahmoodzadeh 2009; Saak et al. 2004), and as a result, there are many yield stress related studies being undertaken in cement and concrete (Moller et al. 2009). Indeed, yield stress has played an important role in many products—for example, colloidal suspensions, foams, polymer gels, concentrated emulsions and composites—in suspending and maintaining shape.

In the literature, both indirect and direct measurement methods have been used to obtain a yield stress. An indirect method is achieved either by fitting shear stress-shear rate data into rheological models, notably Bingham, Casson, and

✉ Ernest E. S. Ong
ernest.e.s.ong@gmail.com

¹ School of Engineering and Information Technology, the University of New South Wales, Canberra, ACT 2600, Australia

Herschel-Bulkley rheological models or by extrapolating shear stress to a zero shear rate directly, where a yield stress is obtained. A direct method involves either the measurement of the shear stress required to initiate a flow or the amount of shear stress recovered from a stopped flow. The latter is conventionally known as the stress relaxation method that measures a dynamic yield stress. A static yield stress is more applicable in our daily lives and it also has a much greater industrial importance. For instance, we are more interested in the forces needed to initiate flow for crude oil in pipelines than the forces recovered as a result of the aging process after stopping the flow. In this paper, the phrase “yield stress” is actually referring to static yield stress.

It has been about a hundred years (Coussot 2017) since Bingham and Green (1919) first proposed the existence of yield stress in their research with paint. They were among the earliest to bring forward the concept of yield stress in fluids. In Bingham’s follow-up publication (Bingham 1922), a popular rheological model (later known as Bingham’s model) that constitutes a yield stress was suggested. Although the model was not presented explicitly (Bingham 1922), Bingham mooted the idea of a linear relationship between shear rate and shear stress in a plastic solid with a yield stress. Since then, for about a century, many have worked on YSFs and their measurement. Nguyen et al. (2006) initiated the first international inter-laboratory study in measuring the yield stress of colloidal TiO_2 at varying concentrations in an aqueous solution. This effort involved a total of six laboratories from Australia, Canada, France, the USA, and Japan using a wide range of direct (vane technique (Dzuy and Boger 1985; Dzuy and Boger 1983), slotted plate technique (Zhu et al. 2001), cylindrical penetrometer technique (Uhlherr et al. 2002)) and indirect methods in measuring or estimating the yield stress of colloidal TiO_2 suspensions. From their measurement results, it was found that the yield stress values obtained were not reproducible among different laboratories, although a much better repeatability was observed within any given laboratory. In their conclusion, they highlighted the need to standardize sample preparation and conditioning procedure to obtain a reliable yield stress value. Stokes and Telford (2004) attempted to measure the yield stress of a thixotropic lamellar gel-structured cream with the vane technique. From their results, the yield stress values obtained are highly dependent on the length of measurement time. They highlighted the difficulty of selecting the most appropriate test procedure for yield stress measurement. In a more recent publication, yield stress measurements were conducted on both simple (non-thixotropic) and thixotropic YSFs by Dinkgreve et al. (2016). The simple YSFs measured include castor oil-in-water emulsions, Carbopol gels, commercial hair gel, and shaving foams. For the thixotropic YSFs, they measured castor oil-in-water emulsions with 2 wt% bentonite clay. Various methods including steady and oscillatory shear measurements were employed in

their yield stress measurement. They concluded that different measurement methods gave significantly different yield stress values for both simple and thixotropic YSFs.

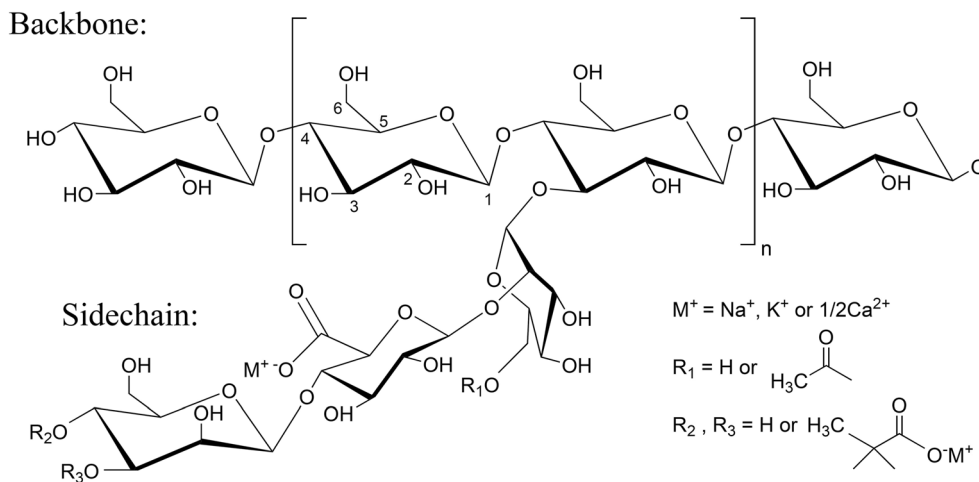
Despite the importance of yield stress, so far there is still no widely recognized or established standard for yield stress measurement (Bonn and Denn 2009; Dinkgreve et al. 2016; Donley et al. 2018). As is commonly known, yield stress measurements are deemed to be inconsistent or difficult. The yield stress measurement of a thixotropic colloid is considered to be even more challenging since the thixotropic behavior gives rise to time-dependent rheological properties (Coussot 2014; Ewoldt and McKinley 2017). The understanding of yield stress should allow a more accurate description in constitutive equations that could predict the flow of materials (Ong et al. 2013). Here in this paper, we have attempted to measure the yield stress of a thixotropic colloid via both direct and indirect measurement methods.

Materials and methods

Xanthan gum (XG) solution was selected as a thixotropic colloid for yield stress measurement because it is widely used in industrial, food, and pharmaceutical applications. The XG consists of repeating penta-saccharide units with a cellulosic backbone (Fig. 1) and it is produced by bacterium *Xanthomonas campestris* (Ong et al. 2018). It has been regarded as the most commercially important microbial polysaccharide (Garcia-Ochoa et al. 2000) for its superior performance in controlling sedimentation, modifying viscosity, reducing drag, and maintaining shape. The applications of XG (Garcia-Ochoa et al. 2000; Moscovici 2015; Petri 2015) include canned soups, jams, sauces, juice drinks, beers, mayonnaise, toothpaste, abrasives, adhesives, explosives, oil well drilling muds, and laundry and agricultural chemicals. Due to its biodegradability and biocompatibility, XG is used in a wide range of biomedical applications (Petri 2015). The number of publications and patents involving XG has also been rising over the years (Petri 2015). Given its broad usage and increasing popularity, XG solution is considered to be a good candidate for our experiments as a general representative of the thixotropic colloids.

The XG (Sigma-Aldrich) that we purchased was used as received. Deionized water was used in preparing XG solutions after a 0.45 μm filtration. The XG solutions were stirred for at least 12 h with a magnetic stirrer in a closed container and kept in a refrigerator for a day at 4 °C before being used in our experiments. In order to make sure that good stability exists in the XG solutions, the zeta potential of a 1 g/L XG solution was measured using a Laser Doppler velocimetry (Zetasizer Nano ZS, Malvern equipment) and the zeta potential was measured to be < -60 mV in all three measurements. Since it is known that the stability of a hydrocolloid such as XG solution improves with increasing concentration (Dickinson 2009;

Fig. 1 The structure of XG (Ong et al. 2018)



Thonart et al. 1985), there should be no concern over polymer aggregation and sedimentation in the more concentrated 0.4, 0.6, 0.8, and 1 wt% XG solutions. The intrinsic viscosity of XG was measured using a Cannon-Ubbelohde viscometer and the measurement was conducted in a water bath at 25 °C. Eight dilute concentrations of XG ranging from 0.4 to 1.0 g/dl were prepared and their respective efflux times were measured five times for each concentration. Using the Rao equation (Rao 1993), as displayed in Eq. (1), where $[\eta]$ is the intrinsic viscosity, η_r is the relative viscosity, and $a = 1/\phi_M$ (ϕ_M is the maximum volume fraction that particles can pack in a suspension), the intrinsic viscosity of XG was obtained as 55.11 dl/g that is close to the reported value in the literature (Brunchi et al. 2014), which also used Sigma-Aldrich XG without salt addition. The Rao equation is particularly suitable for polyelectrolyte solutions such as XG solutions since it considers the polymer swelling behavior and polymer-solvent interactions (Brunchi et al. 2014; Rao 1993). With the addition of 0.1 M NaCl, the intrinsic viscosity of XG was obtained as 24.68 dl/g in our measurement using the Rao equation, and the molecular weight (M_r) of XG can then be estimated through the Mark-Houwink equation (Brunchi et al. 2014; Casas et al. 2000; Milas et al. 1985), as shown in Eq. (2), and from which it is estimated to be 1.916×10^6 g/mol. A Malvern Kinexus Pro rheometer was used in all of our rheological measurements and all of our experiments were conducted at 25 °C. According to the specification given by Malvern, the minimum shear rate and shear stress that can be achieved by our rheometer are $7.5 \times 10^{-8} \text{ s}^{-1}$ and 0.003 Pa, respectively, with a 40 mm plate-plate (PP) configuration and a 2 mm gap between the plates.

$$\frac{1}{2(\eta_r^{1/2}-1)} = \frac{1}{c[\eta]} - \frac{a-1}{2.5} \tag{1}$$

$$[\eta] = 1.7 \cdot 10^{-4} \cdot \langle M_r \rangle^{1.14} \tag{2}$$

Wall slip investigation

Prior to our yield stress measurement, we conducted an investigation on wall slip to minimize measurement errors arising from wall slip. It is commonly known that wall slip is likely to take place, especially in a multi-phase system (Masalova et al. 2008), when a rheological measurement is conducted at low shear rates and smooth shearing geometries are used with a small gap in between. In our strain-controlled measurements, as shown in Fig. 2, wall slip was observed when smooth geometries of a cone-plate (CP) or plate-plate (PP) configuration were used. The wall slip is prevalent at low shear rates and diminishes when the shear rate increases. At a higher shear rate, where a yield stress is exceeded and the dispersed phase (XG polymers) has gained sufficiently high momentum

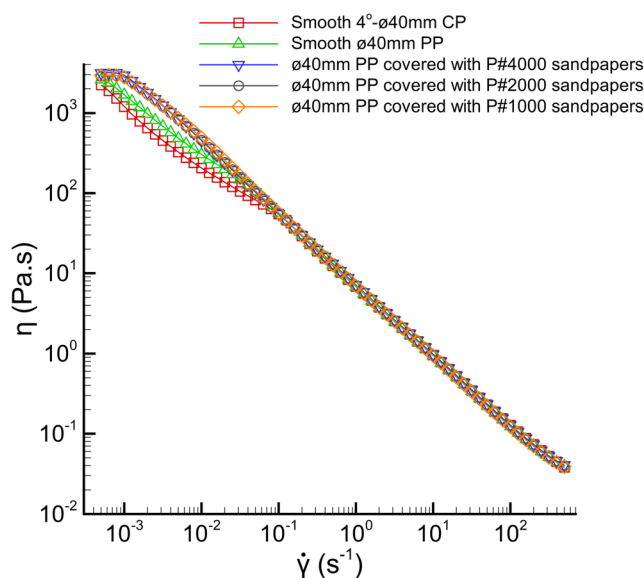


Fig. 2 The shear viscosity (η) of a 1 wt% xanthan gum (XG) solution was measured with an increasing shear rate ($\dot{\gamma}$). Three measurements were done for each configuration. The error bars are not displayed since they are smaller than the symbols

to overcome the physico-chemical forces arising from the wall depletion effect (Barnes 1995; Meeker et al. 2004), the dispersed phase starts to flow together with the continuous phase (water) (Bonn and Denn 2009). As a result, the viscosity gradient is diminished across the solution and the wall slip becomes completely negligible at higher shear rates (Barnes 1995). Wall slip can be expected in a two-phase system, due to the displacement of the dispersed phase from smooth solid geometries, and forms a viscosity gradient at the solid boundaries. Sandpaper-covered plates, however, show either none or less prominent wall slip. The reason is that the sandpaper-covered plates allow the dispersed phase to penetrate into the porous surface, and a more homogeneous solution can exist within the effective gap of these plates. Figure 3 gives a detailed graphical illustration of the above discussions.

The common rough surfaces used to eliminate wall slip include serrated plates, sand-blasted plates, and sandpaper-covered plates. Of these three, sandpaper-covered plates provide a more economical and versatile option. The vane geometry is another viable option to remove wall slip effectively, but it requires a significantly larger amount of sample for a rheological measurement. In the literature, it is reported that the wall slip error can also be minimized by modifying the surface chemistry or the wettability of shearing geometries (Paredes et al. 2015). In our study, there is no significant difference in the rheological measurements by using sandpapers of different grain size. This clearly shows that a secondary flow (Carotenuto and Minale 2013) induced by the porous surface of sandpaper did not take place in the study, even when the roughest sandpaper P#1000 with an average grain size of 18 μm was used. The P#4000 sandpaper with an average grain size of 5 μm was selected in our subsequent rheological measurements.

Thixotropic behavior

Given that there are some conflicting views with regard to the thixotropic behavior of XG solutions in the literature, we

conducted rheological measurements to verify whether the XG solutions are either thixotropic or shear-thinning fluids. In the literature, XG solutions were considered to be shear-thinning fluids (Bewersdorff and Singh 1988; Comba and Sethi 2009; Rochefort and Middleman 1987; Zhong et al. 2013) by some researchers, while others reported them as thixotropic fluids (Benmouffok-Benbelkacem et al. 2010; Carnali 1991; Morris 1977; Tian et al. 2015).

In between the rheological properties of thixotropic and shear-thinning fluids, there is one distinct difference in their dependency on shear history. The shear viscosity of a thixotropic fluid is time-dependent but this is not the case for a shear-thinning fluid. Currently, the generally accepted definition of thixotropy is, according to Mewis and Wagner (2009), the continuous decrease of viscosity with time when a finite shear is applied to a sample that has been previously at rest and the subsequent recovery of viscosity in time when the shear is decreased or arrested. To verify the thixotropic behavior of the XG solutions, the hysteresis technique was used by ramping up and down the shear rates between 0.1 and 100 s^{-1} with 2 min each ramp, as shown in Fig. 4. The rheological responses of mayonnaise (Woolworths Homebrand) and glycerol (Gold Cross) were also measured as references. It is widely recognized that mayonnaise is a thixotropic fluid and a hysteresis loop is expected with the measurement. For glycerol, a Newtonian fluid, no changes in shear viscosity are anticipated under different shear rates. In the figure, hysteresis loops are clearly seen across all XG concentrations studied and this indicates thixotropic behavior. As expected, a hysteresis loop is observed with mayonnaise while glycerol displays a constant shear viscosity across the shear rates studied.

Another method using stepwise changes in shear rates was also employed to verify the thixotropic behavior of the XG solutions. Under strain-controlled measurement as shown in Fig. 5a, the shear rate was suddenly stepped up and down and the transient response in shear stress, as shown in Fig. 5b, was recorded. For a thixotropic fluid, its signature rheological response is the recovery of shear stress in a stepping-down of shear rate (Mewis and Wagner 2009). As displayed in Fig. 5b,

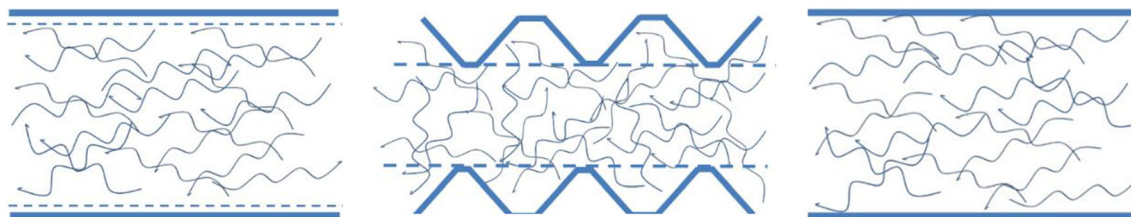


Fig. 3 (Left) An inhomogeneous sample fluid with thin and low-viscosity layers adjacent to the smooth surfaces, as shown by dashed lines. The wavy lines represent the dispersed phase. (Center) The dispersed phase is allowed to “penetrate” the roughened walls and this has created a more homogeneous sample fluid within the dashed lines. The dashed lines show the effective gap between the two rough surfaces.

(Right) The thin and low-viscosity layers, next to the smooth surfaces, start diminishing after a yield stress is exceeded. The dispersed phase is able to get near to the smooth surfaces after overcoming physico-chemical forces at the solid surface and creating a more homogeneous sample fluid as it flows together with the continuous phase. (The above figures are only for illustration and they are not to scale.)

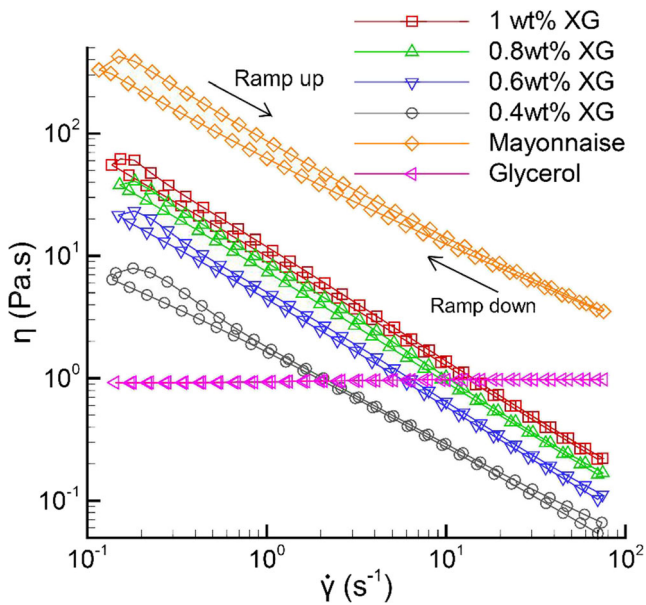


Fig. 4 An evaluation of the thixotropic behavior was carried out by ramping the shear rate ($\dot{\gamma}$) up and down (between 0.1 and 100 s^{-1}) with 2 min each ramp. The error bars are not shown since they are smaller than the symbols

there is a stress overshoot when the XG solutions, initially at rest, were sheared at a constant shear rate of 0.1 s^{-1} . In the literature, a similar stress overshoot was also observed in XG solutions at low shear rates (Ross-Murphy 1995). This stress overshoot under a constant shear rate is one of the characteristics displayed by YSFs and some researchers considered the maximum shear stress recorded in the stress overshoot as yield stress (Bonn et al. 2017). A second stress overshoot is observed when the imposed shear rate is instantaneously increased to 100 s^{-1} . Unlike the first stress overshoot, the corresponding shear stress after the second stress overshoot increases slightly and displays a relatively constant value, while the shear stress decreases gradually in the aftermath of the first

stress overshoot. When the shear rate is rapidly decreased to 1 s^{-1} , the shear stress responds with a stress undershoot and subsequently increases with the rebuilding of polymeric network until it reaches an equilibrium. The recovery of shear stress displayed in the XG solutions during the stepping-down of shear rate has clearly shown a thixotropic behavior. Across all of the XG solutions studied with different XG concentrations, a similar pattern of rheological responses is observed.

Time independence test

A comprehensive time independence test was conducted to obtain an optimum stress relaxation time and from there, a yield stress could be measured. The time independence test here refers to the experimental examination of the minimum stress relaxation time required, in such a way that the accuracy of a yield stress measurement is not greatly affected by the ongoing aging process within a thixotropic colloid at rest. Failure to conduct a comprehensive time independence test may lead to inconsistencies in the yield stress measurement of a thixotropic colloid. Since shear history is a concern for thixotropic colloids, the information of an optimum stress relaxation time is necessary to ensure that the YSFs are well recovered from the imposed forces during sample loading. To ensure all our samples were pre-sheared similarly during our sample loading, a 3 ml syringe was used in the sample loading to maintain the consistency of the loaded sample.

Before the time independence test was conducted using small amplitude oscillatory shear (SAOS) measurement, a frequency sweep was carried out to determine the linear viscoelastic region. It was found that the yield stress, which was assumed to take place at the maximum storage modulus, is largely independent of angular frequency under a SAOS measurement ($< 15\%$ strain amplitude) as long as the angular

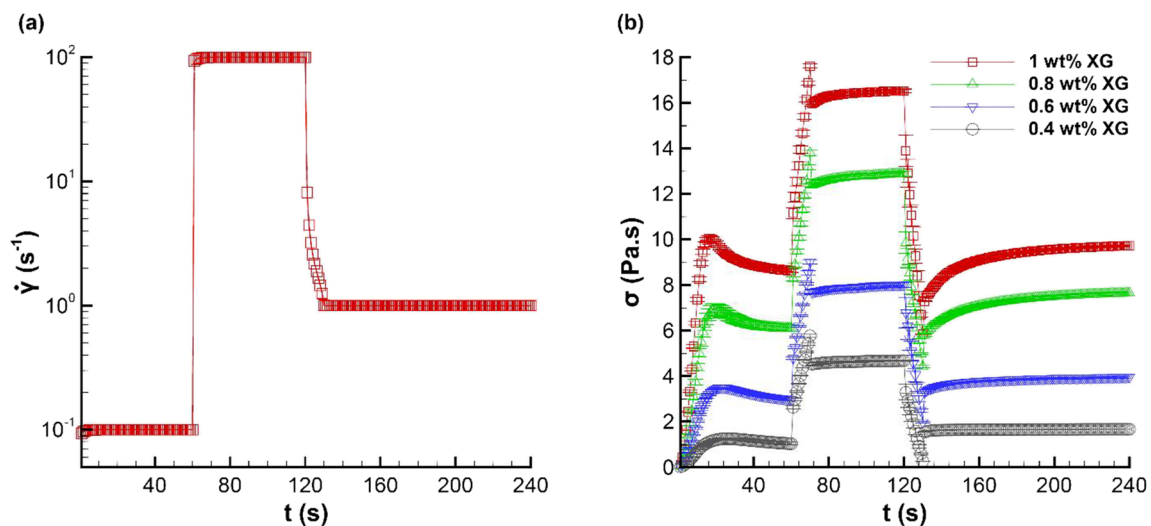


Fig. 5 **a** Stepwise changes in shear rate applied to the tested sample. **b** The transient shear stress (σ) response of the XG solutions under stepwise changes in shear rate ($\dot{\gamma}$)

frequency is low (≤ 1.5 Hz) and within the linear viscoelastic region, where both the storage modulus G' and loss modulus G'' are in plateaus and $G' > G''$. In a SAOS measurement, the shear stress $\sigma(t)$ can be determined through Eq. (3), where γ_0 is the shear strain, ω is the angular frequency, and t is time. Equation (3) can also be represented in an alternative form, as shown in Eq. (4), under the linear responses of small deformations, where G^* is the complex modulus ($|G^*| = |G' + iG''|$) and δ is the phase angle. Figure 6 shows the SAOS measurement of the 1 wt% XG using different angular frequencies. It is known in the literature (Ross-Murphy 1995) that XG solutions display the characteristics of a weak gel system, in which $G' > G''$ and both moduli G' and G'' are largely independent of angular frequency. Unlike strong gels, XG solutions flow without fracture under large deformations and display a recovery of solid (gel-like) character (Ross-Murphy 1995).

$$\sigma(t) = \gamma_0 \left[G'(\omega) \sin(\omega t) + G''(\omega) \cos(\omega t) \right] \quad (3)$$

$$\sigma(t) = \gamma_0 |G^*| \sin(\omega t + \delta) \quad (4)$$

From the time independence test (as shown in Table 1), the yield stress values that were taken at the maximum G' are found to be increasing over time. The SAOS measurement was conducted five times for each test and the statistical uncertainty is calculated based on the standard deviation of these five measurements. After 45 min of stress relaxation time, the yield stress value was found to be increasing marginally with less than 1% difference between 45 and 65 min, which is also well within the margin of error in the measurements. Since the stress relaxation time is reasonably expected to reduce with a much lower XG concentration, the 45-min stress relaxation time was selected and used in our subsequent experiments of

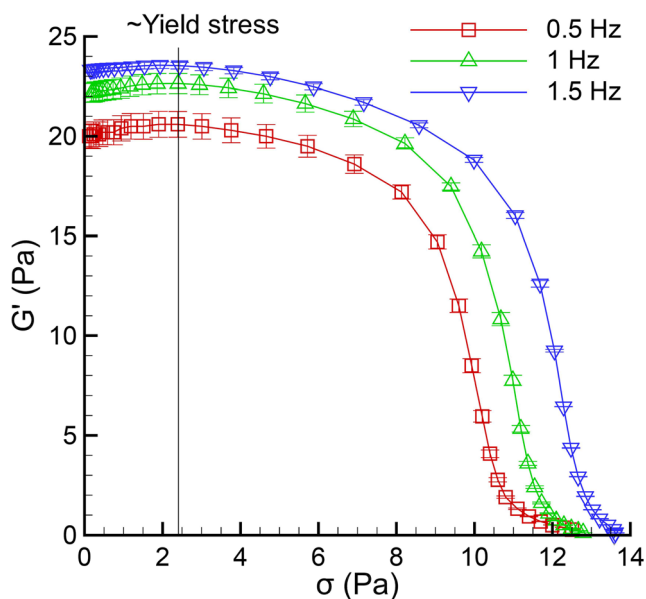


Fig. 6 SAOS measurements of the 1 wt% XG solution under different angular frequencies

Table 1 A time independence test for 1 wt% XG solution

Stress relaxation time (minutes)	Yield stress (Pa)
1	2.12 ± 0.03
10	2.17 ± 0.05
25	2.28 ± 0.03
45	2.40 ± 0.04
65	2.41 ± 0.04

≤ 1 wt% XG solutions. The long timescale required (> 1 h) for a complete stress relaxation of a 1 wt% XG solution with the addition of 0.02 M KCl and 0.02% NaN_3 was also reported by Richardson and Ross-Murphy (1987).

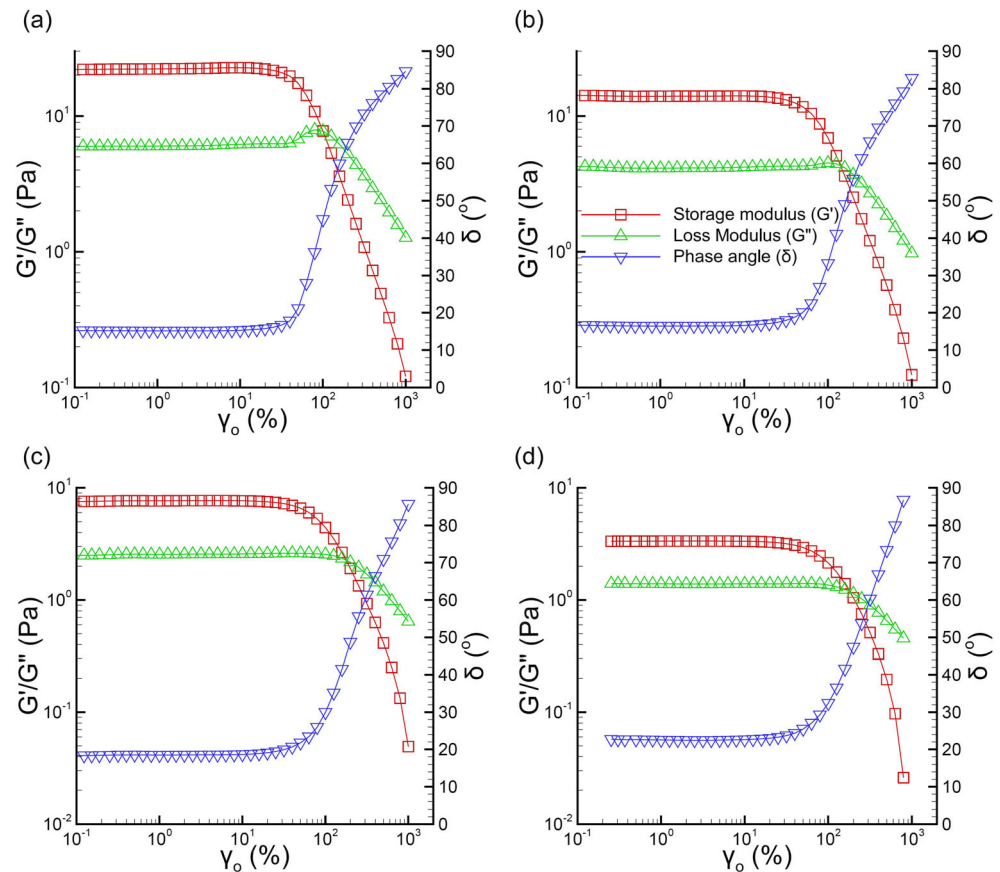
Results and discussion

Oscillatory shear measurement

In our strain-controlled oscillatory shear measurement, five measurements were conducted using 1 Hz angular frequency with an increasing strain amplitude for each XG concentration studied. As shown in Fig. 7, both G' and G'' are in plateaus under the double logarithmic plot when the strain amplitude is small. At the start of decreasing G' , possibly after a yield stress is exceeded, the phase angle starts increasing. After G'' reaches a peak (Fig. 10), it eventually starts decreasing but at a much slower rate than G' since the viscous behavior is more dominant at a higher deformation rate. The strain overshoot behavior, as displayed in the G'' , is evident in 1 wt% XG solution. Song et al. (2006b) and Hyun et al. (2002) also discovered a similar behavior with ≥ 1 wt% XG solutions. In lower XG concentrations, this strain overshoot phenomenon is less evident. It is believed that this strain overshoot behavior is caused by the formation of structured complexes (Hyun et al. 2002; Song et al. 2006b) or liquid crystalline structure (Richardson and Ross-Murphy 1987) in highly concentrated XG solutions. When the strain amplitude keeps increasing up to 1000%, the phase angle also rises beyond 80° and this indicates a very viscous liquid.

As compared to the steady shear measurement, SAOS measurement is found to be advantageous since its non-destructive nature at small deformations only causes minimum disturbance to the fluid structure responsible for its yield behavior (Nguyen and Boger 1992). In the literature, there are various ways suggested to determine a yield stress from SAOS measurements (Donley et al. 2018) but a consensus has not been reached on the accepted way of determining a yield stress from the SAOS measurements. In our current study, a yield stress was obtained at (I) the characteristic modulus, where $G' = G''$ (Walls et al. 2003); (II) the crossover point between the small- and large-amplitude responses in G' (Dinkgreve

Fig. 7 The response of storage modulus G' , loss modulus G'' , and phase angle δ in the oscillatory shear measurement of **a** 1 wt%, **b** 0.8 wt%, **c** 0.6 wt%, and **d** 0.4 wt% XG solutions under 1 Hz angular frequency with an increasing strain amplitude $\gamma_o(\%)$



et al. 2016; Rouyer et al. 2005); (III) the maximum G' (Castro et al. 2010; Walls et al. 2003); (IV) the maximum G'' (Donley et al. 2018); and (V) the crossover point between the small- and large-amplitude responses in the stress amplitude (Dinkgreve et al. 2016; Saint-Jalmes and Durian 1999). Figures 8, 9, 10, and 11 show the plots of SAOS measurement data in an attempt to extract a yield stress, and Table 2 lists the yield stresses obtained via these methods. These methods imply the solid-to-liquid transition occurs at a point after which a material starts flowing. As shown in Table 2, all methods give relatively similar yield stress values in all concentrations of XG solution studied, except for method III that consistently gives the lowest yield stress value. Among all the methods used in obtaining a yield stress, methods I, III, and IV can provide a definite value of yield stress, whereas methods II and V are dependent on the range of data measured and the quality of the power-law fitting.

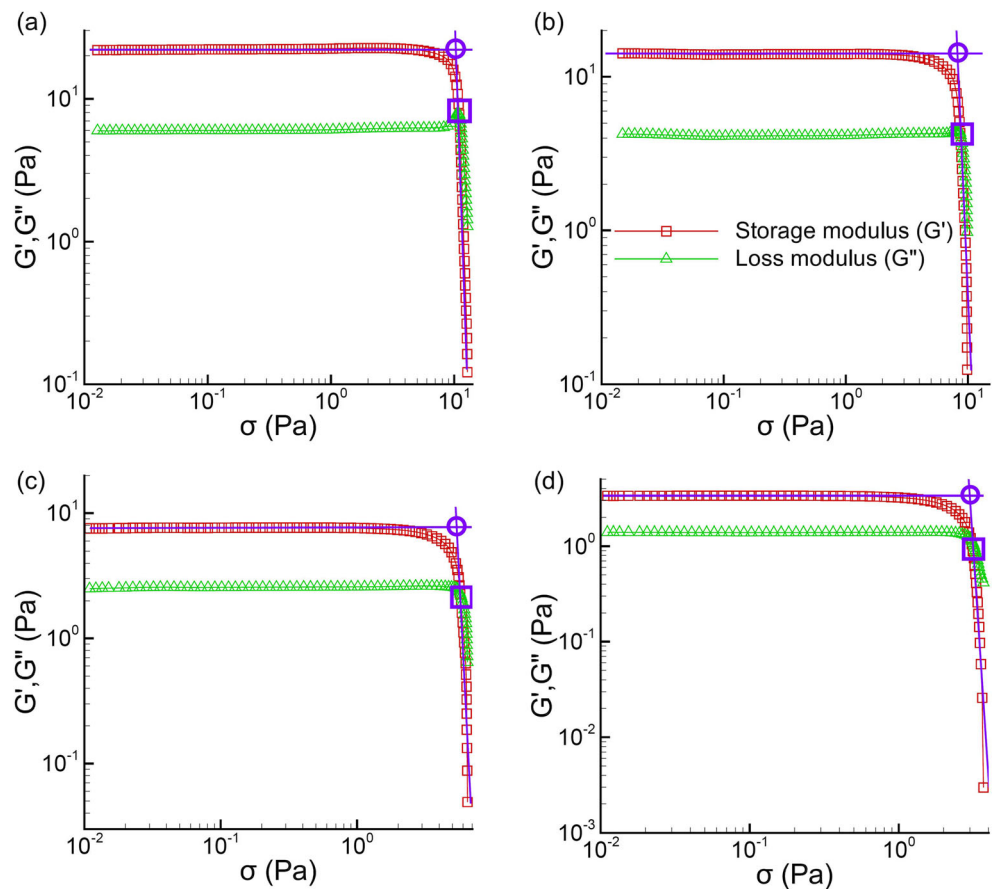
Steady shear measurement

In our stress-controlled steady shear measurement, four different lengths of measurement time were conducted. In Fig. 12, the first Newtonian plateaus at low shear stress rise with increasing length of measurement time across all the XG solutions studied. In the past, the first Newtonian plateau at low shear stress was once used as a counterargument (Barnes

1999) for the existence of a yield stress since it points to a finite viscosity that could indicate a flowing fluid. Nevertheless, this is clearly not the case since the observed Newtonian plateau is time-dependent and not at a steady state (Dinkgreve et al. 2017; Malkin et al. 2017). As displayed in Fig. 13, the first Newtonian plateau is expected to rise with the increasing length of measurement time. The solid lines, as shown in the figure, are the power-law fittings. A rising power of time in the power-law fittings of the first Newtonian plateau over measurement time is expected with the increasing concentration of XG. In the literature, the apparent first Newtonian plateau of YSFs was also found to be increasing indefinitely with measurement time (Coussot et al. 2002; Møller et al. 2009). This displays a solid-like behavior where there is no finite viscosity and the material does not flow. This may also imply that there is no finite shear stress below a critical shear rate. Therefore, this is not a question of Deborah number, as suggested by Reiner (1964), which indicates that everything may flow under an infinitesimal force if the time of observation is sufficiently long (Coussot 2017).

Even though the apparent first Newtonian plateau increases over time in our measurements, the shear viscosity in the power-law region matches very well across the different lengths of measurement time. From Fig. 12 alone, it is rather difficult to judge the point beyond which the material starts to flow. Therefore, we have plotted the percentage change of

Fig. 8 An attempt to obtain the yield stress of **a** 1 wt%, **b** 0.8 wt%, **c** 0.6 wt%, and **d** 0.4 wt% XG solutions at the characteristic modulus (as indicated in purple square boxes) and the crossover point (as indicated in circles) between the small- and large-amplitude responses in G' . The solid purple lines are the power-law fittings

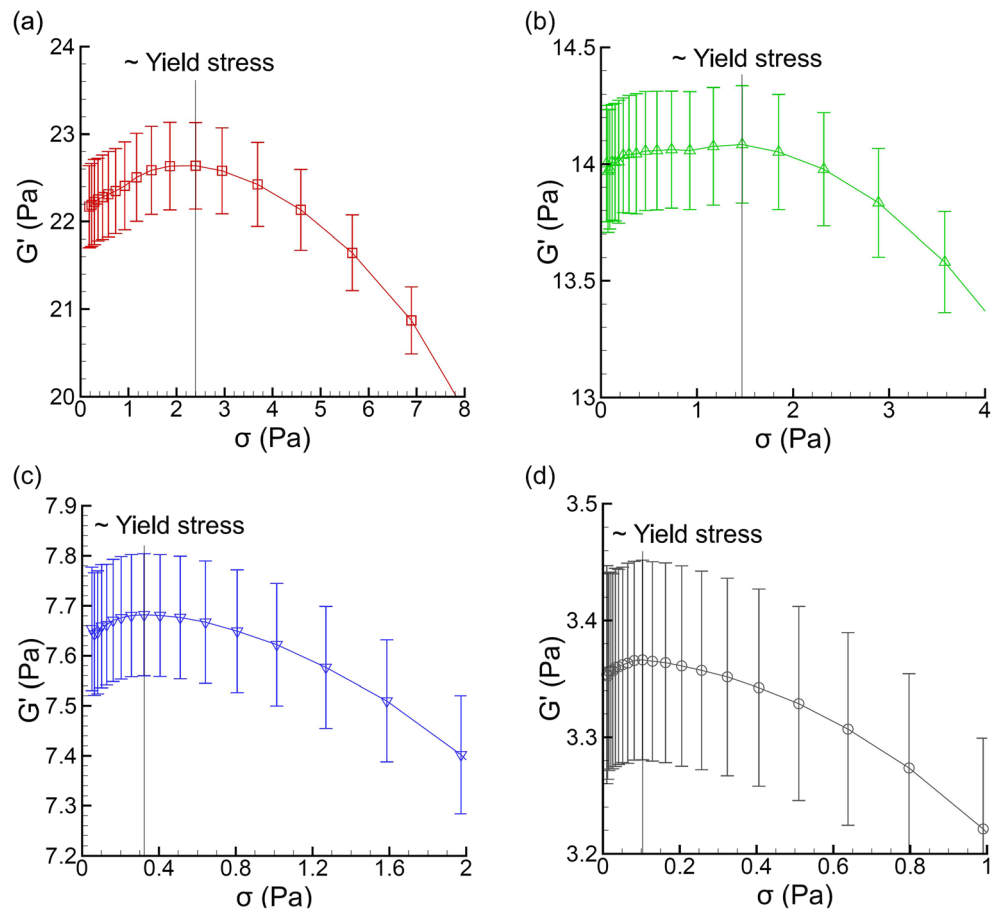


shear viscosity ($\% \Delta \eta$) against shear stress as shown in Fig. 14. In the figure, a possible range of yield stress is shown by the dotted lines. The yield stress is reasonably estimated to take place within a range of shear stresses after which there is a consistent drop in $\% \Delta \eta$. This should indicate a breakdown of microstructures beyond a yield stress. Before the breakdown of microstructures, which leads to an eventual flow, there is an oscillation around the 0% change of apparent shear viscosity. Although the shear stress is steadily increased, the change of the apparent shear viscosity is non-monotonic in the low shear stress region. The first Newtonian plateau, which occurs well before a yield stress is exceeded, is not actually a “plateau” as it seems. Instead, the apparent shear viscosity at the first Newtonian plateau changes elastically in a state of equilibrium before a yield stress is exceeded. After a yield stress is exceeded, shear rejuvenation becomes more dominant than the aging of microstructures (Møller et al. 2006), and this leads to a large drop in shear viscosity or an avalanche of flow (Coussot et al. 2002). Figure 14 shows that the 3-h measurement has the steepest percentage drop in shear viscosity, followed by 2-h, 1-h, and 30-min measurements. This is a reasonable outcome since more shearing time was spent at each data point in the 3-h measurement and thus the avalanche behavior (Coussot et al. 2002; Møller et al. 2009) is more prominent. Despite different lengths of measurement time,

all of our measurements point to a similar possible range of shear stresses at which a yield stress could take place, and a uniform downward trend is displayed after the XG solution starts flowing. When the shear stress keeps increasing, the percentage change of shear viscosity reaches a minimum and increases as it approaches the second Newtonian plateau at a higher shear stress.

The solid-like behavior of XG solutions is dependent on a network of polymer entanglements (Pelletier et al. 2001), which is formed through the hydrodynamic and excluded volume interactions between the polymer chains as concentration increases, without which the solution will flow like a viscous liquid under shear. The associative nature of XG polymer makes a high viscosity solution, even at a low XG concentration. Our new graphical method (Fig. 14) uncovers an interesting phenomenon that shows a resistance to the avalanche of flow when the shear stress is steadily increased. This avalanche of flow refers to the acceleration of flow as observed in the YSFs (Coussot et al. 2002; Møller et al. 2009). In the conventional shear stress-shear rate and shear viscosity-shear rate graphs, such a resistance cannot be observed clearly since the power-law region ($\eta \propto \dot{\gamma}^{n-1}$) displays as a straight line in a double logarithmic plot. The coefficient of determination (R^2) is > 0.97 for a power law fitting in the power-law region

Fig. 9 An attempt to obtain the yield stress of **a** 1 wt%, **b** 0.8 wt%, **c** 0.6 wt%, and **d** 0.4 wt% XG solutions at the maximum G'

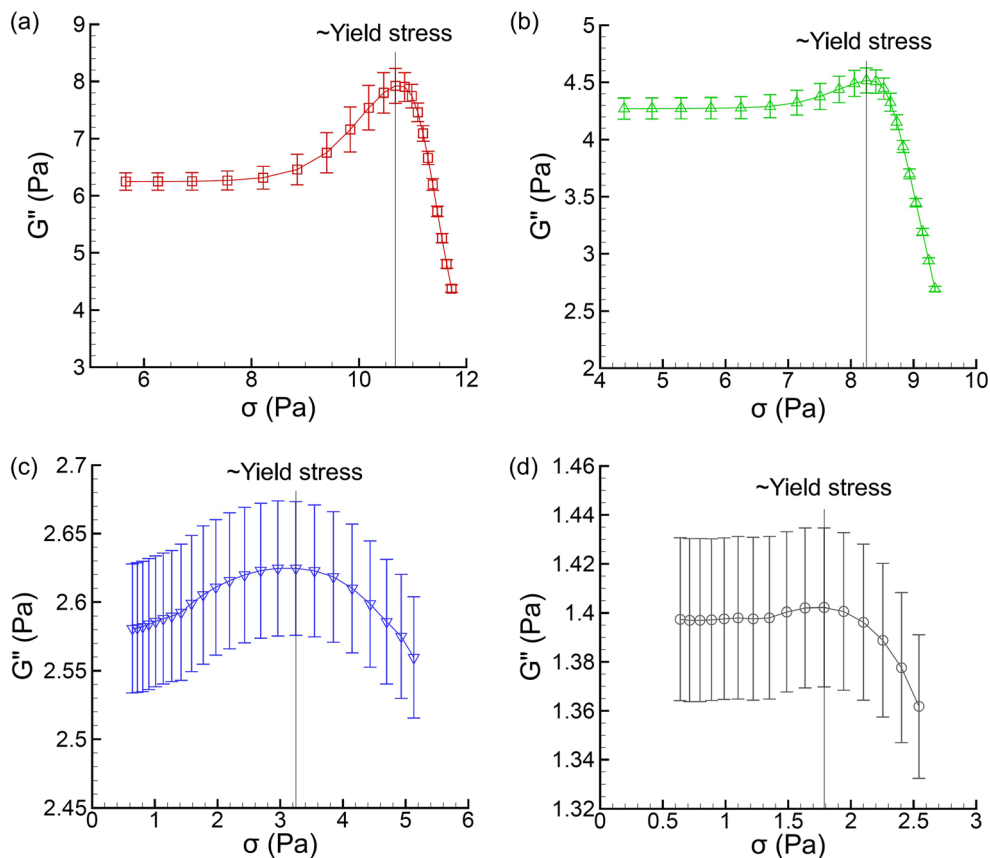


for all of the XG solutions. The resistance is clearly displayed in the XG solutions, in which the strongest resistance is observed in the less concentrated 0.4 and 0.6 wt% XG solutions. In the 1 wt% XG solution, the resistance is minimal since it is only observed in both of the 2-h and 3-h measurements. This minimal resistance observed in the concentrated 1 wt% XG solution could be due to the formation of a liquid crystalline structure with ordered conformation (Lee and Brant 2002; Lim et al. 1984; Livolant and Bouligand 1986; Pelletier et al. 2001), and thus it is less susceptible to a conformational change under shear.

The observed resistance to the avalanche of flow is likely caused by a shear-induced conformational transition. Although there are some debates on the ordered conformation of XG, most researchers (Gulrez et al. 2012) agree that the ordered conformation is a coaxial double helix, while the disordered conformation is a random flexible coil. The helical conformation can be achieved by adding salt into a dilute aqueous XG solution, and it is always accompanied by a reduction of viscosity (Pelletier et al. 2001). This is due to a reduction of the hydrodynamic volume in the helical conformation with the tri-saccharide side chains folding back to the cellulosic backbone (Morris et al. 1977; Pelletier et al. 2001). For the coiled conformation, it has extended side chains that

enable more extensive non-covalent bonding with other polymer chains, which increases the resistance to shear. However, when the shear stress is continually increased, the polymer chains will progressively be more aligned in the direction of flow and thus the resistance to shear decreases. A similar phenomenon could also happen in the XG solutions when the resistance to the avalanche of flow subsides with increasing shear stress. As is commonly known, the conformational change of XG polymer can be obtained by altering the XG concentration, temperature, salinity, as well as the acetyl and pyruvate content (Gulrez et al. 2012; Lee and Brant 2002; Milas and Rinaudo 1979; Morris et al. 1977; Pelletier et al. 2001). Our molecular dynamics simulation studies also show a more extended conformation of XG oligomer as the temperature rises (Ong et al. 2018). In their studies of microfluidization with XG, Lagoueyte and Paquin (1998) postulated that the helix-coil transition can be achieved by shear deformation. To date, there is still very limited work being done to understand the conformational change of XG under shear. However, in the research of DNA polymers (LeDuc et al. 1999; Smith et al. 1999), which share some similar structural and chemical characteristics with XG polymers (Livolant 1986; Livolant and Bouligand 1986; Maurstad et al. 2007; Tinland and Rinaudo 1989), the conformational change took

Fig. 10 An attempt to obtain the yield stress of **a** 1 wt%, **b** 0.8 wt%, **c** 0.6 wt%, and **d** 0.4 wt% XG solutions at the maximum G''



place in the shear rate range of 0.05 to 4.0 s^{-1} . The range of shear rates coincides very well with the shear rates (0.06–

2.7 s^{-1}), where the resistance to the avalanche of flow is observed in the XG solutions.

Model fitting

Other than using direct yield stress measurements, an indirect approach such as model fitting can also be employed to obtain a yield stress. In the literature, the classical rheological models such as Bingham, Casson, and Herschel-Bulkley models have been used to obtain a yield stress by fitting the shear stress-shear rate data. However, there are some drawbacks in employing these rheological models since they are highly dependent on the range of shear stress-shear rate data measured and they do not present a complete rheological description (such as thixotropy and avalanche behavior (Denn and Bonn 2011)) of YSFs. For XG solutions, as studied by Song et al. (2006a), the shear stress-shear rate data of concentrated XG solutions (≥ 1 wt%) is found well fitted to Herschel-Bulkley, Heinz-Casson (Heinz 1959), and Mizrahi-Berk (Mizrahi and Berk 1972) models at shear rates above 0.04 s^{-1} . In the current study, we attempted to fit the shear stress-shear rate data of the XG solutions into various rheological models, as displayed in Eqs. (5)–(9). Figure 15 shows the fitting of these rheological models using the Levenberg-Marquardt algorithm for shear rates between 0.1 and 1000 s^{-1} . A good agreement is observed between our measurement data and these rheological models

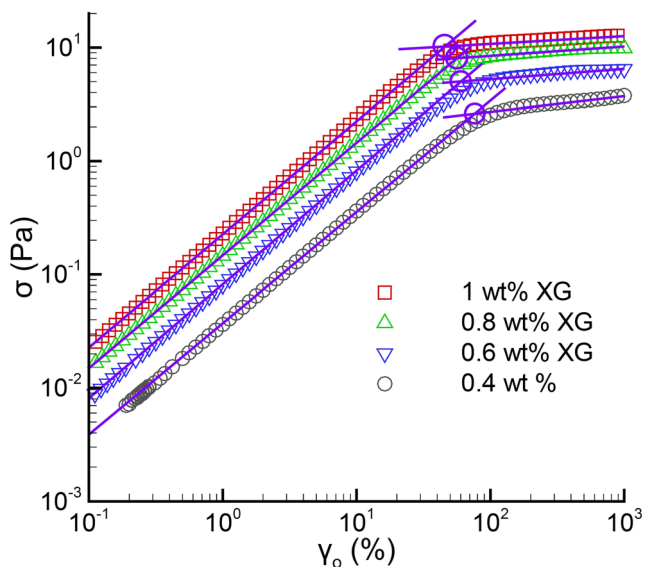


Fig. 11 An attempt to obtain the yield stress of 1 wt%, 0.8 wt%, 0.6 wt%, and 0.4 wt% XG solutions at the crossover point (as indicated in circles) between the small- and large-amplitude responses in the stress amplitude. The solid purple lines are the power-law fittings

Table 2 Determination of a yield stress from SAOS data points using different methods

Concentration of XG (wt%)	Yield stress (Pa) ¹				
	I	II	III	IV	V
1	10.98 ± 0.17	10.47 ± 0.16	2.40 ± 0.04	10.71 ± 0.20	10.55 ± 0.26
0.8	8.63 ± 0.04	8.00 ± 0.03	1.47 ± 0.03	8.25 ± 0.04	8.19 ± 0.12
0.6	5.71 ± 0.06	5.16 ± 0.05	0.33 ± 0.02	3.19 ± 0.08	5.32 ± 0.14
0.4	3.04 ± 0.04	2.84 ± 0.05	0.11 ± 0.01	1.79 ± 0.04	2.78 ± 0.04

¹“I” represents the yield stress obtained at the characteristic modulus, $G' = G''$. “II” represents the yield stress obtained at the crossover point between the small- and large-amplitude responses in G' . “III” represents the yield stress obtained at the maximum G' . “IV” represents the yield stress obtained at the maximum G'' . “V” represents the yield stress obtained at the crossover point between the small- and large-amplitude responses in the stress amplitude

with the $R^2 > 0.95$ in all XG concentrations studied. Nonetheless, from the figure, it is also clear to see that these models cannot fit the shear stress-shear rate data very well at low shear rates ($< 0.1 \text{ s}^{-1}$). Table 3 lists the yield stress values estimated using various rheological models. The standard deviation is calculated based on the yield stress values obtained from the shear stress-shear rate data of our 30-min, 1-h, 2-h, and 3-h steady shear measurements. As shown in the table, Herschel-Bulkley, Heinz-Casson, and Mizrahi-Berk models obtained relatively similar values of yield stress, while Bingham and Casson models estimated the highest and lowest

yield stress value, respectively, across all XG concentrations studied.

$$\text{Bingham} : \sigma = \sigma_y + k\dot{\gamma} \tag{5}$$

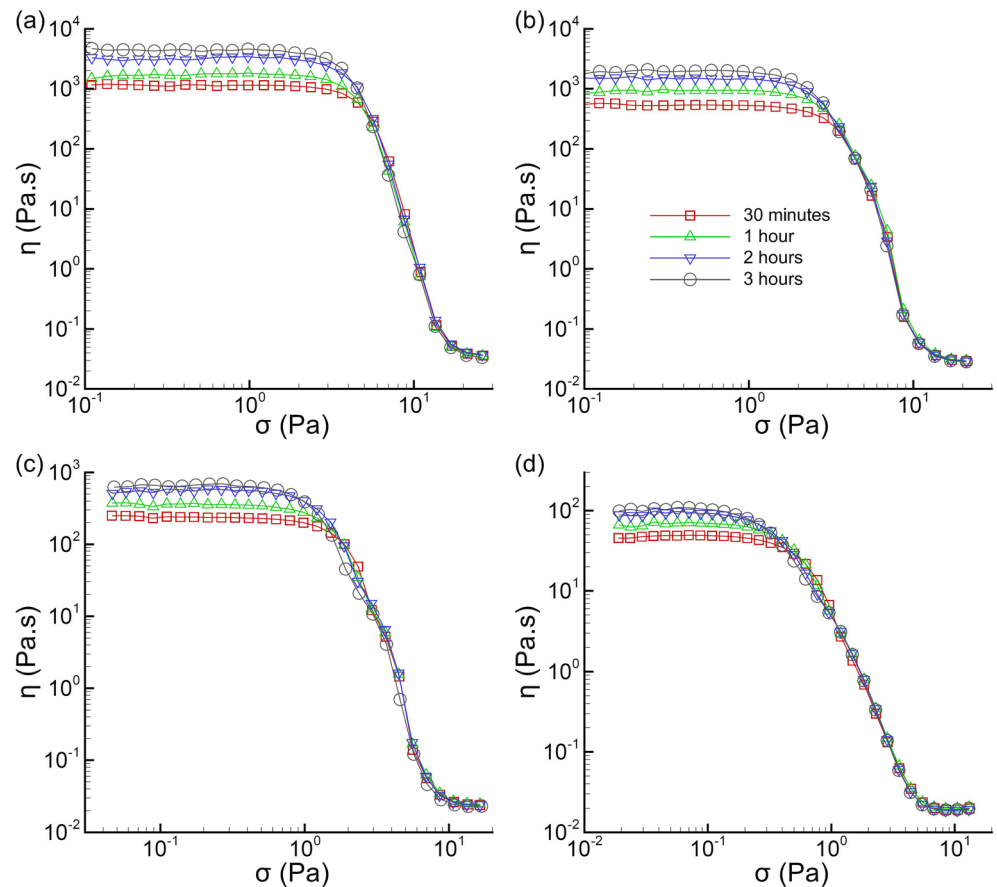
$$\text{Casson} : \sqrt{\sigma} = \sqrt{\sigma_y} + k\sqrt{\dot{\gamma}} \tag{6}$$

$$\text{Herschel-Bulkley} : \sigma = \sigma_y + k\dot{\gamma}^n \tag{7}$$

$$\text{Heinz-Casson} : \sigma^n = \sigma_y^n + k\dot{\gamma}^n \tag{8}$$

$$\text{Mizrahi-Berk} : \sqrt{\sigma} = \sqrt{\sigma_y} + k\dot{\gamma}^n \tag{9}$$

Fig. 12 The stress-controlled steady shear measurement of **a** 1 wt%, **b** 0.8 wt%, **c** 0.6 wt%, and **d** 0.4 wt% XG solutions under different lengths of measurement time



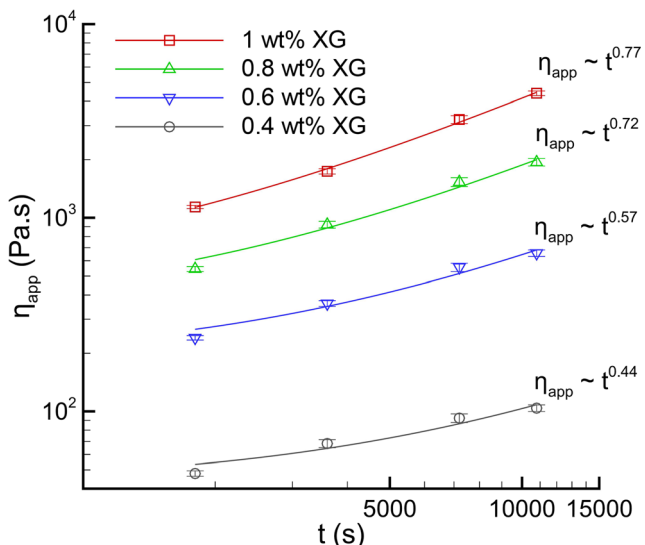


Fig. 13 The apparent shear viscosity of the first Newtonian plateau η_{app} for 1 wt%, 0.8 wt%, 0.6 wt%, and 0.4 wt% XG solutions with an increasing length of measurement time

In order to obtain an unambiguous yield stress value from our steady shear measurement data, we attempted to fit the shear viscosity-shear stress data of the XG solutions using the complementary error function (CEF) that is well suited for data with a characteristic sigmoidal curve. The equation

for the CEF is shown in Eq. (10), where $C_1, C_2, C_3,$ and C_4 are constants, and the derivative of the equation is shown in Eq. (11). In a double-logarithmic shear viscosity-shear stress plot, as displayed in Fig. 16, the XG solutions display the first and second Newtonian plateaus at low and high shear stresses, respectively, and the curve of our experimental shear viscosity-shear stress data can resemble a sigmoidal curve. In the figure, the solid lines show that the CEF fits very well in the first Newtonian and power-law regions but not so in the high shear stress region, since the function consistently underestimates the second Newtonian plateau. Figure 17 shows the derivatives of the CEF fitted to our steady shear measurement data. The derivatives are zero at both ends of shear stresses since the apparent shear viscosity of the XG solutions is relatively constant in the first and second Newtonian plateaus. The 3-h measurement displays the steepest curve gradient, given that the avalanche of flow is the most prominent with the longest shearing time at each of the data points in our 3-h steady shear measurement. Table 4 lists the yield stress obtained at the drop of 1% from the maximum shear viscosity (the first Newtonian plateau) using the CEF. The standard deviation is calculated based on the yield stress values obtained from our 30-min, 1-h, 2-h, and 3-h steady shear measurements. The assumption of a yield stress taking place at a drop of 1% from the maximum shear viscosity allows the

Fig. 14 The percentage change in shear viscosity ($\% \Delta \eta$) with an increasing shear stress (σ) for **a** 1 wt%, **b** 0.8 wt%, **c** 0.6 wt%, and **d** 0.4 wt% XG solutions under different lengths of measurement time. The dotted lines indicate the possible range of shear stresses at which a yield stress could take place

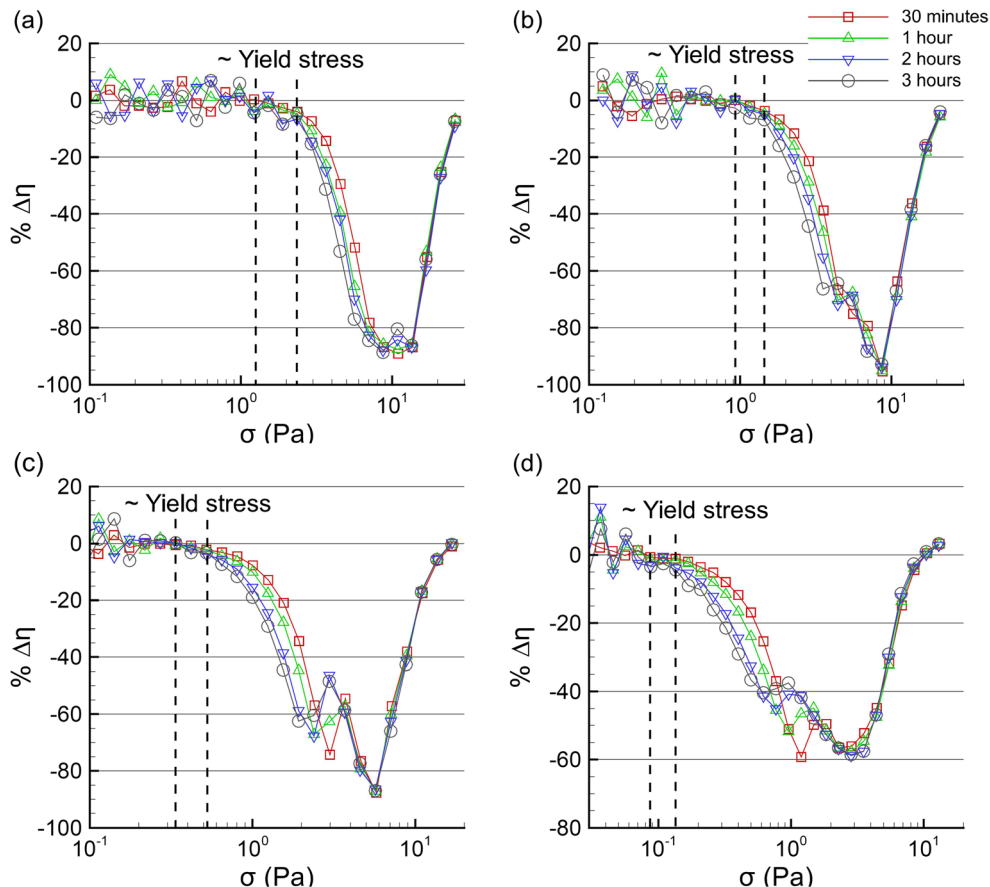
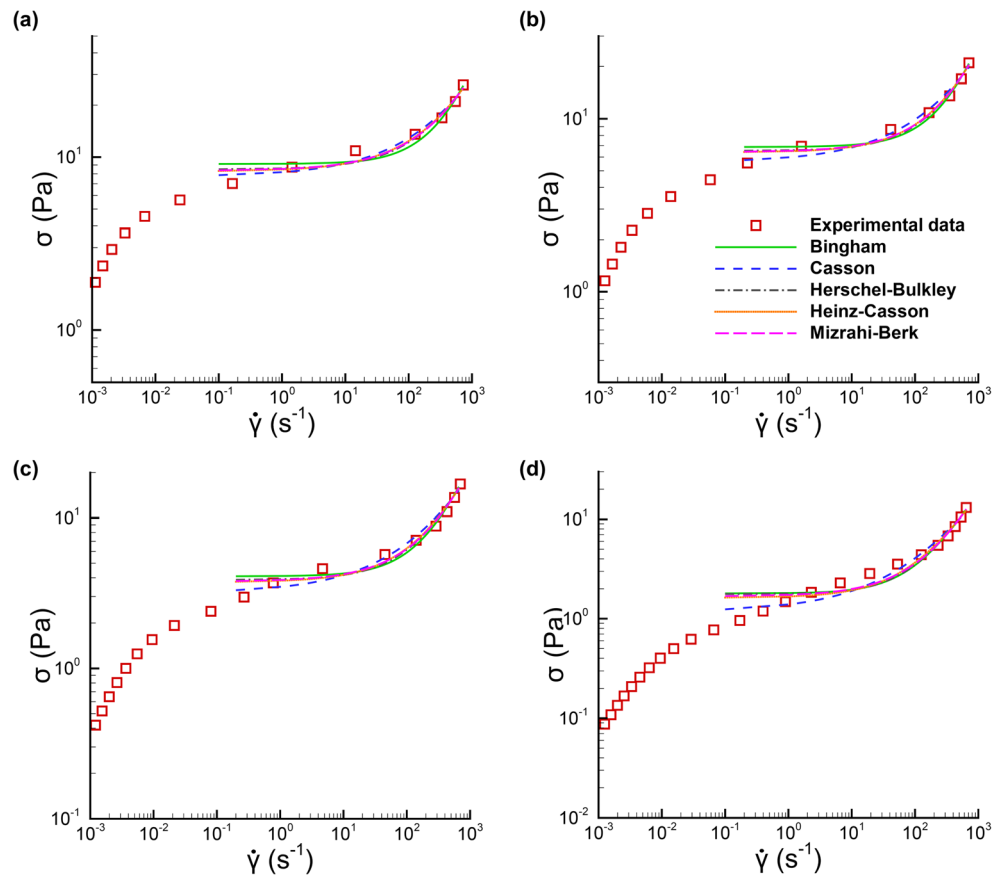


Fig. 15 Fitting of the shear stress (σ)–shear rate ($\dot{\gamma}$) data for **a** 1 wt%, **b** 0.8 wt%, **c** 0.6 wt%, and **d** 0.4 wt% XG solutions using various rheological models at $0.1 < \dot{\gamma} < 1000 \text{ s}^{-1}$



determination of an unambiguous yield stress value from our steady shear measurement. However, it does not necessarily mean that the material should flow beyond the drop of 1% from the first Newtonian plateau, since its purpose is to obtain a yield stress from steady shear measurements without ambiguity, and to provide a platform for comparing yield stresses obtained using steady shear measurements.

$$y = \frac{2C_1}{\sqrt{\pi}} \int_{-(C_2x+C_3)}^{\infty} e^{-t^2} .dt + C_4 \tag{10}$$

$$\frac{dy}{dx} = -\frac{2C_1C_2e^{-(C_2x+C_3)^2}}{\sqrt{\pi}} \tag{11}$$

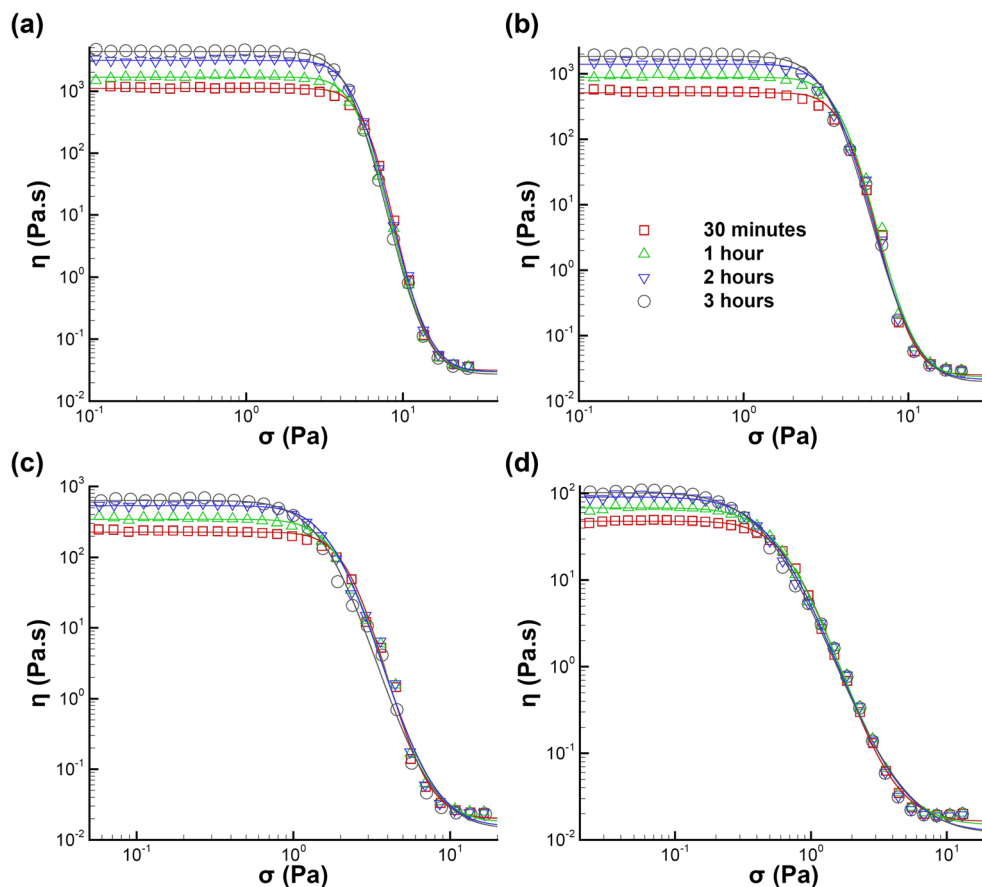
Creep test

To further verify the accuracy of the yield stress values obtained via both oscillatory and steady shear measurements, creep tests were conducted by employing various constant shear stresses and each creep test was run for 50 min. The creep test is capable of showing the range of shear stresses that a yield stress should take place. However, the test may only serve as a supplementary measurement at best since it cannot measure a yield stress precisely and sometimes it is rather difficult to judge whether a material truly flows or not, especially when the applied shear stress is close to a yield stress. In such a case, a much longer creep time may be required to get a more conclusive result but this risks a loss of solvent that may lead to inaccurate results. In a creep test, if a yield stress is not

Table 3 The yield stress of XG solutions obtained via the fitting of various rheological models with shear rates between 0.1 and 1000 s^{-1}

Concentrations of XG (wt%)	Yield stress (Pa)				
	Bingham	Casson	Herschel-Bulkley	Heinz-Casson	Mizrahi-Berk
1	9.22 ± 0.09	7.82 ± 0.10	8.44 ± 0.09	8.19 ± 0.11	8.28 ± 0.10
0.8	6.76 ± 0.07	5.47 ± 0.09	6.51 ± 0.01	6.40 ± 0.01	6.41 ± 0.01
0.6	4.04 ± 0.06	3.11 ± 0.09	3.90 ± 0.05	3.78 ± 0.06	3.81 ± 0.05
0.4	1.78 ± 0.03	1.16 ± 0.02	1.76 ± 0.01	1.62 ± 0.02	1.67 ± 0.01

Fig. 16 Curve fitting of the double logarithmic plot of η and σ using CEF for **a** 1 wt%, **b** 0.8 wt%, **c** 0.6 wt%, and **d** 0.4 wt% XG solutions



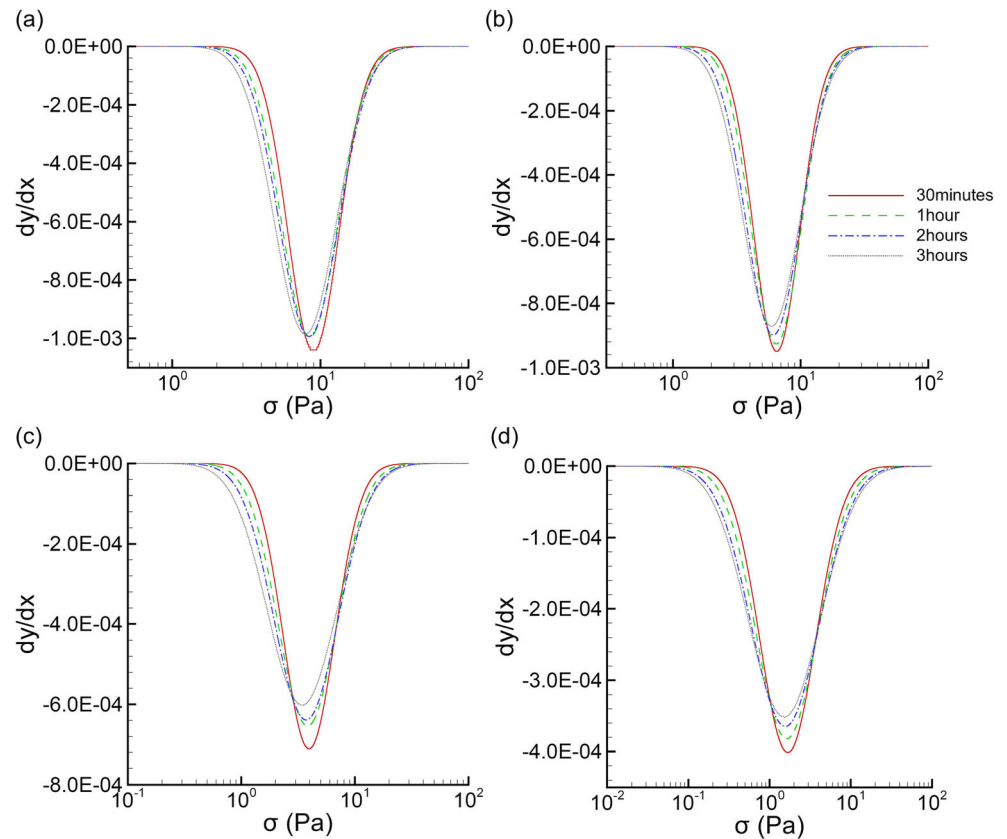
exceeded under an applied shear stress, a material should behave as if it is an elastic solid, in which the shear viscosity increases indefinitely with time. However, the material should flow with a decreasing shear viscosity (for shear-thinning and thixotropic materials) when a yield stress is exceeded.

In Fig. 18a, the shear viscosity of the 1 wt% XG solution seems to increase indefinitely with a relatively constant rate under 1 and 2 Pa shear stresses. When it is subjected to 4 and 5 Pa shear stresses, the shear viscosity decreases and this indicates that the solution flows. Unlike the 1 and 2 Pa shear stresses, the shear viscosity increases but with a declining rate when it is under a constant shear stress of 3 Pa. It is rather hard to judge whether a flow would eventually take place at 3 Pa but it is clear to see that the yield stress of 1 wt% XG solution should fall between 2 and 4 Pa. In Fig. 18b, the shear viscosity of the 0.8 wt% XG solution seems to increase indefinitely under shear stresses of 0.5 and 1 Pa. When it is subjected to 2 Pa shear stress, the shear viscosity increases with a decreasing rate, in which the shear viscosity could possibly drop if a much longer measurement time is conducted. Under a constant 3 Pa shear stress, the shear viscosity is found to increase slightly and remains relatively constant over the course of the 50-min creep test.

The shear viscosity decreases, however, when it is under 4 Pa shear stress and remains relatively constant after 10 min of creep test. From the creep test results, the yield stress of 0.8 wt% XG solution should possibly fall within the range of 1 and 3 Pa.

In Fig. 18c, the shear viscosity of 0.6 wt% XG solution drops more than 50% from its initial shear viscosity when it is subjected to a constant shear stress of 2 Pa and stays relatively constant after 700 s of creep test. The shear viscosity increases by more than 30% when 1 Pa shear stress is applied and remains largely the same when the creep test runs beyond 500 s. However, when it is subjected to 0.1 and 0.2 Pa shear stresses, the shear viscosity seems to be increasing indefinitely with time. Under a constant shear stress of 0.7 Pa, the shear viscosity increases at a decreasing rate. From the creep test results, the yield stress of 0.6 wt% XG solution should possibly fall within the range of 0.2 and 1 Pa. In Fig. 18d, the shear viscosity of 0.4 wt% XG solution drops by roughly 50% when 1 Pa shear stress is applied in the course of the 50-min creep test. When it is subjected to 0.3 and 0.5 Pa shear stresses, the shear viscosity increases initially but decreases as the solution starts to flow. The shear viscosity, nonetheless, rises indefinitely under the shear stresses of 0.02 and 0.05 Pa. From the creep test results, the yield stress of 0.4 wt% XG solution should possibly fall within the range of 0.3 and 0.05 Pa.

Fig. 17 The changes in the curve gradient of the CEF (as plotted in Fig. 16) for **a** 1 wt%, **b** 0.8 wt%, **c** 0.6 wt%, and **d** 0.4 wt% XG solutions



Summary

In this paper, we measured the yield stress of aqueous XG solutions in different XG concentration. In our SAOS measurements, various methods were attempted to obtain a yield stress. Except for the yield stress obtained at the maximum \dot{G} , the yield stress obtained using other methods exceeds the range of yield stress determined in both steady shear and creep tests. In the steady shear measurements, a possible range of yield stress was determined using the plot of the percentage change of shear viscosity ($\% \Delta \eta$) against shear stress (Fig. 14). The possible range of yield stress is selected before a consistent drop in $\% \Delta \eta$ and that should indicate fluid flow. A resistance to an avalanche of flow is clearly observed in the 0.4 and 0.6 wt% XG solutions but less evident in the more highly

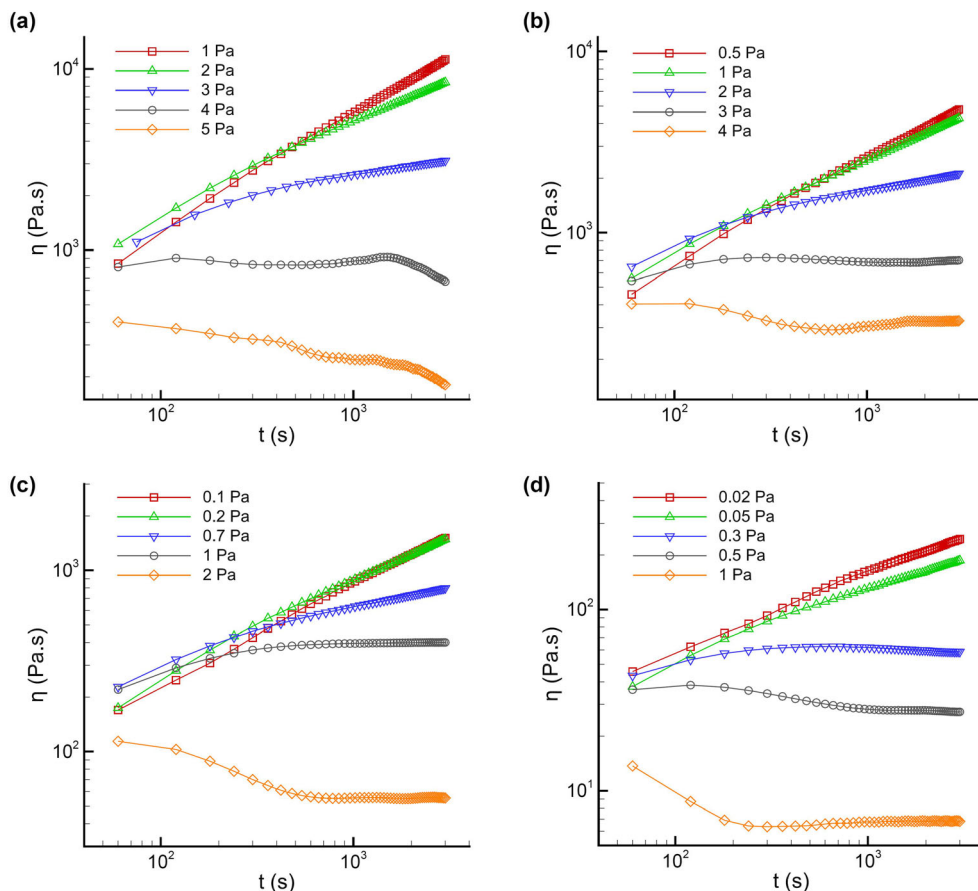
concentrated 0.8 and 1 wt% XG solutions. The resistance observed in the semi-concentrated XG solutions is likely due to a conformational change of XG polymers under shear, as observed in DNA polymers. In the more highly concentrated XG solutions, the conformational change is likely deterred by the existence of a liquid crystalline structure with ordered conformation (Lee and Brant 2002; Lim et al. 1984; Livolant and Bouligand 1986; Pelletier et al. 2001). Nevertheless, further investigations should be conducted to verify this finding.

We also attempted to obtain a yield stress by fitting shear stress-shear rate data into various rheological models. There are drawbacks in using the indirect measurement method via model fitting because the models do not provide a complete rheological description of YSFs and the yield stress value obtained is highly dependent on the range of measurement data. Using the steady shear measurement data within the shear rates of 0.1 to 1000 s^{-1} , the yield stress value obtained using five different rheological models (Bingham, Casson, Herschel-Bulkley, Heinz-Casson and Mizrahi-Berk) exceeds the range of yield stress determined in both steady shear and creep tests. To get an ambiguous yield stress value from our steady shear measurements, the shear viscosity-shear stress data is fitted using the CEF since the double-logarithmic shear viscosity-shear stress plot of aqueous XG solutions can

Table 4 The determination of a yield stress from our steady shear measurement data via the fitting of CEF

Concentration of XG (wt%)	Yield stress (Pa)
1	2.11 ± 0.37
0.8	1.47 ± 0.27
0.6	0.57 ± 0.14
0.4	0.11 ± 0.04

Fig. 18 Creep test of **a** 1 wt%, **b** 0.8 wt%, **c** 0.6 wt%, and **d** 0.4 wt% aqueous XG solutions



resemble a characteristic sigmoidal curve. A yield stress is obtained from the CEF by assuming that the yield stress is at the drop of 1% in shear viscosity from the first Newtonian plateau. This assumption allows an ambiguous yield stress value to be obtained in steady shear measurements and helps to create a platform to compare the yield stress obtained by researchers. We also conducted creep tests to determine the range of yield stress for the aqueous XG solutions.

Table 5 shows the comparison of yield stresses obtained using various methods. In the table, it shows that the yield stress obtained at the maximum G' in SAOS measurements is well within the range of yield stress determined in both steady shear and creep tests. The yield stress obtained using the CEF (at the drop of 1% in shear viscosity from the first Newtonian plateau) also matches well with the range of yield

stress and shows good agreement with the yield stress obtained at the maximum G' in SAOS measurements. Despite different views in determining a yield stress, we found that a yield stress can be taken reliably and conveniently at the maximum G' in a SAOS measurement. Since the solid-like elastic response of YSFs is directly related to G' , the consistent decline of G' after the maximum G' could indicate flow of materials.

Conclusion

We have successfully demonstrated many possible ways of measuring the yield stress of a thixotropic colloid and concluded that the most accurate and reliable way is to conduct

Table 5 A comparison of yield stresses obtained using various methods

Concentration of XG (wt%)	Yield stress (Pa)			
	Steady shear	Creep test	CEF	At maximum G'
1	1.2–2.4	2–4	2.11 ± 0.37	2.40 ± 0.04
0.8	0.9–1.5	1–4	1.47 ± 0.27	1.47 ± 0.03
0.6	0.3–0.6	0.2–2	0.57 ± 0.14	0.33 ± 0.02
0.4	0.08–0.14	0.05–0.3	0.11 ± 0.04	0.11 ± 0.01

SAOS measurements, from which a yield stress can be obtained conveniently at the maximum \dot{G}' . To conclude our current experimental investigations on the yield stress measurement of a thixotropic colloid, we have listed out the important steps in conducting a reliable yield stress measurement as follows:

1. Firstly, a standard sample loading procedure should be conducted (Nguyen et al. 2006) because it is important to ensure the initial sample deformation arising from the sample loading is consistent. In this study, a 3 ml syringe was employed in the sample loading and the yield stress measurement results were very consistent across all XG concentrations studied (< 0.05 Pa difference in the shear stress obtained at the maximum \dot{G}').
2. Secondly, a thorough wall slip investigation should be conducted to avoid any measurement error arising from wall slip. Alternatively, the vane technique (Dzuy and Boger 1985) can be employed to solve the wall slip problem.
3. Thirdly, a comprehensive time independence test should be conducted to determine the optimal stress relaxation time required for the loaded sample to recover from the imposed forces during sample loading.
4. Lastly, SAOS measurements should be conducted under a low angular frequency (i.e., ≤ 1.5 Hz) and a fresh sample should be used in each run to maintain the rheological consistency of the loaded sample.

From our current experimental investigation, it is found that the use of the existing rheological models cannot give a reliable yield stress value due to their poor ability to correlate with the experimental data in the low shear rate region ($< 0.1 \text{ s}^{-1}$) and the inherent complexity of time-dependent rheological properties that cannot be addressed by current rheological models. However, these rheological models are still able to give a reasonable estimation of the rheological properties at higher shear rates ($0.1\text{--}1000 \text{ s}^{-1}$). Future investigations should focus on formulating new rheological models that can sufficiently address the unique rheological properties (e.g., elasticity, time-dependent properties, and avalanche behavior) of a thixotropic YSF. In addition, the development of a sophisticated algorithm is also urgently needed to run numerical simulations of YSFs (Saramito and Wachs 2017) and to compute their transport properties accurately for engineering applications.

Acknowledgments We would like to thank Ms. Kate Badek for the use of Malvern Zetasizer Nano ZS. The financial support received from the Australian Government Research Training Program Scholarship is also greatly appreciated.

References

- Balhoff MT, Lake LW, Bommer PM, Lewis RE, Weber MJ, Calderin JM (2011) Rheological and yield stress measurements of non-Newtonian fluids using a marsh funnel. *J Pet Sci Eng* 77:393–402
- Barnes HA (1995) A review of the slip (wall depletion) of polymer solutions, emulsions and particle suspensions in viscometers: its cause, character, and cure. *J Non-Newtonian Fluid Mech* 56:221–251
- Barnes HA (1999) The yield stress—a review or ‘*παντα ρει*’—everything flows? *J Non-Newtonian Fluid Mech* 81:133–178
- Barnes H, Walters K (1985) The yield stress myth? *Rheol Acta* 24:323–326
- Benmouffok-Benbelkacem G, Caton F, Baravian C, Skali-Lami S (2010) Non-linear viscoelasticity and temporal behavior of typical yield stress fluids: Carbopol, xanthan and ketchup. *Rheol Acta* 49:305–314
- Bewersdorff H-W, Singh R (1988) Rheological and drag reduction characteristics of xanthan gum solutions. *Rheol Acta* 27:617–627
- Bingham EC (1922) Fluidity and plasticity, vol 2. McGraw-Hill Book Compny, Incorporated, New York City
- Bingham E, Green H (1919) Paint, a plastic material and not a viscous liquid; the measurement of its mobility and yield value. In: *Proc. am. Soc. test. Mater*, pp 640–664
- Bonn D, Denn MM (2009) Yield stress fluids slowly yield to analysis. *Science* 324:1401–1402
- Bonn D, Denn MM, Berthier L, Divoux T, Manneville S (2017) Yield stress materials in soft condensed matter. *Rev Mod Phys* 89:035005
- Botha J et al (2016) A novel technology for complex rheological measurements. In: WM2016 conference proceedings. WM Symposia, Tempe
- Brunchi C-E, Morariu S, Bercea M (2014) Intrinsic viscosity and conformational parameters of xanthan in aqueous solutions: salt addition effect. *Colloids Surf B: Biointerfaces* 122:512–519
- Carnali J (1991) A dispersed anisotropic phase as the origin of the weak-gel properties of aqueous xanthan gum. *J Appl Polym Sci* 43:929–941
- Carotenuto C, Minale M (2013) On the use of rough geometries in rheometry. *J Non-Newtonian Fluid Mech* 198:39–47
- Casas J, Santos V, Garcia-Ochoa F (2000) Xanthan gum production under several operational conditions: molecular structure and rheological properties☆. *Enzym Microb Technol* 26:282–291
- Castro M, Giles D, Macosko C, Moaddel T (2010) Comparison of methods to measure yield stress of soft solids. *J Rheol* (1978-present) 54:81–94
- Chang C, Nguyen QD, Rønningsen HP (1999) Isothermal start-up of pipeline transporting waxy crude oil. *J Non-Newtonian Fluid Mech* 87:127–154
- Chidiac S, Mahmoodzadeh F (2009) Plastic viscosity of fresh concrete—a critical review of predictions methods. *Cem Concr Compos* 31:535–544
- Comba S, Sethi R (2009) Stabilization of highly concentrated suspensions of iron nanoparticles using shear-thinning gels of xanthan gum. *Water Res* 43:3717–3726
- Coussot P (2014) Yield stress fluid flows: a review of experimental data. *J Non-Newtonian Fluid Mech* 211:31–49
- Coussot P (2017) Bingham’s heritage. *Rheol Acta* 56:163–176
- Coussot P, Nguyen QD, Huynh H, Bonn D (2002) Avalanche behavior in yield stress fluids. *Phys Rev Lett* 88:175501
- Denn MM, Bonn D (2011) Issues in the flow of yield-stress liquids. *Rheol Acta* 50:307–315
- Dickinson E (2009) Hydrocolloids as emulsifiers and emulsion stabilizers. *Food Hydrocoll* 23:1473–1482
- Dinkgreve M, Paredes J, Denn MM, Bonn D (2016) On different ways of measuring “the” yield stress. *J Non-Newtonian Fluid Mech* 238:233–241

- Dinkgreve M, Denn MM, Bonn D (2017) “Everything flows?”: elastic effects on startup flows of yield-stress fluids. *Rheol Acta* 56:189–194
- Donley GJ, de Bruyn JR, McKinley GH, Rogers SA (2019) Time-resolved dynamics of the yielding transition in soft materials. *J Non-Newtonian Fluid Mech* 264:117–134
- Dzuy NQ, Boger DV (1983) Yield stress measurement for concentrated suspensions. *J Rheol* (1978-present) 27:321–349
- Dzuy NQ, Boger D (1985) Direct yield stress measurement with the vane method. *J Rheol* (1978-present) 29:335–347
- Ewoldt RH, McKinley GH (2017) Mapping thixo-elasto-visco-plastic behavior. *Rheol Acta* 56:195–210
- García-Ochoa F, Santos V, Casas J, Gomez E (2000) Xanthan gum: production, recovery, and properties. *Biotechnol Adv* 18:549–579
- Gens A, Sánchez M, Guimarães LDN, Alonso EE, Lloret A, Olivella S, Villar MV, Huertas F (2009) A full-scale in situ heating test for high-level nuclear waste disposal: observations, analysis and interpretation. *Géotechnique* 59:377–399
- Gulrez SK, Al-Assaf S, Fang Y, Phillips GO, Gunning AP (2012) Revisiting the conformation of xanthan and the effect of industrially relevant treatments. *Carbohydr Polym* 90:1235–1243
- Heinz W (1959) The Casson flow equation: its validity for suspension of paints. *Mater Prüfung* 1:311–316
- Hyun K, Kim SH, Ahn KH, Lee SJ (2002) Large amplitude oscillatory shear as a way to classify the complex fluids. *J Non-Newtonian Fluid Mech* 107:51–65
- Lagoueyte N, Paquin P (1998) Effects of microfluidization on the functional properties of xanthan gum. *Food Hydrocoll* 12:365–371
- LeDuc P, Haber C, Bao G, Wirtz D (1999) Dynamics of individual flexible polymers in a shear flow. *Nature* 399:564–566
- Lee H-C, Brant DA (2002) Rheology of concentrated isotropic and anisotropic xanthan solutions. 1. A rodlike low molecular weight sample. *Macromolecules* 35:2212–2222
- Lim T, Uhl JT, Prud'homme RK (1984) Rheology of self-associating concentrated xanthan solutions. *J Rheol* (1978-present) 28:367–379
- Livolant F (1986) Cholesteric liquid crystalline phases given by three helical biological polymers: DNA, PBLG and xanthan. A comparative analysis of their textures. *J Phys* 47:1605–1616
- Livolant F, Bouligand Y (1986) Liquid crystalline phases given by helical biological polymers (DNA, PBLG and xanthan). Columnar textures. *J Phys* 47:1813–1827
- Malkin A, Kulichikhin V, Ilyin S (2017) A modern look on yield stress fluids. *Rheol Acta* 56:177–188
- Masalova I, Malkin AY, Foudazi R (2008) Yield stress of emulsions and suspensions as measured in steady shearing and in oscillations. *Appl Rheol* 18:44790
- Maustad G, Danielsen S, Stokke BT (2007) The influence of charge density of chitosan in the compaction of the polyanions DNA and xanthan. *Biomacromolecules* 8:1124–1130
- Meeker SP, Bonnecaze RT, Cloitre M (2004) Slip and flow in soft particle pastes. *Phys Rev Lett* 92:198302
- Mendes R, Vinay G, Coussot P (2016) Yield stress and minimum pressure for simulating the flow restart of a waxy crude oil pipeline. *Energy Fuel* 31:395–407
- Mewis J, Wagner NJ (2009) Thixotropy. *Adv Colloid Interf Sci* 147:148:214–227
- Milas M, Rinaudo M (1979) Conformational investigation on the bacterial polysaccharide xanthan. *Carbohydr Res* 76:189–196
- Milas M, Rinaudo M, Tinland B (1985) The viscosity dependence on concentration, molecular weight and shear rate of xanthan solutions. *Polym Bull* 14:157–164
- Mizrahi S, Berk Z (1972) Flow behaviour of concentrated orange juice: mathematical treatment. *J Texture Stud* 3:69–79
- Møller PC, Mewis J, Bonn D (2006) Yield stress and thixotropy: on the difficulty of measuring yield stresses in practice. *Soft Matter* 2:274–283
- Møller P, Fall A, Bonn D (2009) Origin of apparent viscosity in yield stress fluids below yielding. *EPL (Europhysics Letters)* 87:38004
- Moller P, Fall A, Chikkadi V, Derks D, Bonn D (2009) An attempt to categorize yield stress fluid behaviour. *Philos Trans R Soc Lond A: Math Phys Eng Sci* 367:5139–5155
- Morris E (1977) Molecular origin of xanthan solution properties. In: ACS Symposium Series American Chemical Society
- Morris E, Rees D, Young G, Walkinshaw M, Darke A (1977) Order-disorder transition for a bacterial polysaccharide in solution. A role for polysaccharide conformation in recognition between *Xanthomonas* pathogen and its plant host. *J Mol Biol* 110:1–16
- Moscovici M (2015) Present and future medical applications of microbial exopolysaccharides. *Front Microbiol* 6:1012
- Nguyen Q, Boger D (1992) Measuring the flow properties of yield stress fluids. *Annu Rev Fluid Mech* 24:47–88
- Nguyen QD, Akroyd T, De Kee DC, Zhu L (2006) Yield stress measurements in suspensions: an inter-laboratory study. *Korea-Australia Rheol J* 18:15–24
- Norrman J, Skjæraasen O, Oschmann H-J, Paso K, Sjöblom J (2016) Axial stress localization facilitates pressure propagation in gelled pipes. *Physics of Fluids* (1994-present) 28:033102
- Ong EE, Abdullah M, Loh W, Ooi C, Chan R (2013) FSI implications of EMC rheological properties to 3D IC with TSV structures during plastic encapsulation process. *Microelectron Reliab* 53:600–611
- Ong EE, O’Byrne S, Liow J-L (2018) Molecular dynamics study on the structural and dynamic properties of xanthan gum in a dilute solution under the effect of temperature. In: AIP conference proceedings, vol 1. AIP Publishing, New York, p 030008
- Paredes J, Shahidzadeh N, Bonn D (2015) Wall slip and fluidity in emulsion flow. *Phys Rev E* 92:042313
- Pelletier E, Viebke C, Meadows J, Williams P (2001) A rheological study of the order–disorder conformational transition of xanthan gum. *Biopolymers* 59:339–346
- Petri DF (2015) Xanthan gum: a versatile biopolymer for biomedical and technological applications. *J Appl Polym Sci* 132:42035
- Rao M (1993) Viscosity of dilute to moderately concentrated polymer solutions. *Polymer* 34:592–596
- Reiner M (1964) The Deborah number physics today, vol 17, p 62
- Richardson RK, Ross-Murphy SB (1987) Non-linear viscoelasticity of polysaccharide solutions. 2: xanthan polysaccharide solutions. *Int J Biol Macromol* 9:257–264
- Rocheffort WE, Middleman S (1987) Rheology of xanthan gum: salt, temperature, and strain effects in oscillatory and steady shear experiments. *J Rheol* 31:337–369
- Ross-Murphy SB (1995) Structure–property relationships in food biopolymer gels and solutions. *J Rheol* 39:1451–1463
- Rouyer F, Cohen-Addad S, Höhler R (2005) Is the yield stress of aqueous foam a well-defined quantity? *Colloids Surf A Physicochem Eng Asp* 263:111–116
- Saak AW, Jennings HM, Shah SP (2004) A generalized approach for the determination of yield stress by slump and slump flow. *Cem Concr Res* 34:363–371
- Saint-Jalmes A, Durian DJ (1999) Vanishing elasticity for wet foams: equivalence with emulsions and role of polydispersity. *J Rheol* 43:1411–1422
- Saramito P, Wachs A (2017) Progress in numerical simulation of yield stress fluid flows. *Rheol Acta* 56:211–230
- Smith DE, Babcock HP, Chu S (1999) Single-polymer dynamics in steady shear flow. *Science* 283:1724–1727

- Song K-W, Kim Y-S, Chang G-S (2006a) Rheology of concentrated xanthan gum solutions: steady shear flow behavior. *Fibers Polym* 7:129–138
- Song K-W, Kuk H-Y, Chang G-S (2006b) Rheology of concentrated xanthan gum solutions: oscillatory shear flow behavior. *Korea-Australia Rheol J* 18:67–81
- Stokes J, Telford J (2004) Measuring the yield behaviour of structured fluids. *J Non-Newtonian Fluid Mech* 124:137–146
- Thonart P, Paquot M, Hermans L, Alaoui H, d'Ippolito P (1985) Xanthan production by *Xanthomonas campestris* NRRL B-1459 and interfacial approach by zeta potential measurement. *Enzym Microb Technol* 7:235–238
- Tian M, Fang B, Jin L, Lu Y, Qiu X, Jin H, Li K (2015) Rheological and drag reduction properties of hydroxypropyl xanthan gum solutions. *Chin J Chem Eng* 23:1440–1446
- Tinland B, Rinaudo M (1989) Dependence of the stiffness of the xanthan chain on the external salt concentration. *Macromolecules* 22:1863–1865
- Uhlherr P, Guo J, Fang T-N, Tiu C (2002) Static measurement of yield stress using a cylindrical penetrometer Korea. *Australia Rheol J* 14:17–23
- Walls H, Caines SB, Sanchez AM, Khan SA (2003) Yield stress and wall slip phenomena in colloidal silica gels. *J Rheol (1978-present)* 47:847–868
- Zhong L, Oostrom M, Truex MJ, Vermeul VR, Szecsody JE (2013) Rheological behavior of xanthan gum solution related to shear thinning fluid delivery for subsurface remediation. *J Hazard Mater* 244:160–170
- Zhu L, Sun N, Papadopoulos K, De Kee D (2001) A slotted plate device for measuring static yield stress. *J Rheol* 45:1105–1122

Publisher's note Springer Nature remains neutral with regard to jurisdictional claims in published maps and institutional affiliations.